

TITLE:

Comprehensive investigation of HYPERSCINT RP-FLASH scintillator for electron FLASH research

AUTHORS:

Lixiang Guo^{1*}, Banghao Zhou¹, Yi-Chun Tsai¹, Kai Jiang², Viktor Iakovenko², and Ken Kang-Hsin Wang^{1*}

¹Biomedical Imaging and Radiation Technology Laboratory (BIRTLab), Department of Radiation Oncology, University of Texas Southwestern Medical Center, Dallas, Texas, USA

²Department of Radiation Oncology, University of Texas Southwestern Medical Center, Dallas, Texas, USA

***CORRESPONDENCE:**

Lixiang Guo

Department of Radiation Oncology, University of Texas Southwestern Medical Center, 5323 Harry Hines Blvd., Dallas, TX 75390, USA

Tel: 469-236-9619

Email: lixiang.guo@utsouthwestern.edu

Ken Kang-Hsin Wang, PhD

Department of Radiation Oncology, University of Texas Southwestern Medical Center, 5323 Harry Hines Blvd., Dallas, TX 75390, USA

Tel: 614-282-0859

Email: kang-hsin.wang@utsouthwestern.edu

RUNNING TITLE:

HYPERSCINT RP-FLASH UHDR electron dosimetry

KEY WORDS:

FLASH radiotherapy, ultra-high dose rate, dosimetry, scintillator

ABSTRACT

Background: The normal tissue sparing effect of ultra-high dose rate irradiation (≥ 40 Gy/s, UHDR) has attracted significant research interest for FLASH radiotherapy (RT). Accurate, dose rate independent, fast-response dosimeters capable of resolving the spatiotemporal characteristics of UHDR beams are urgently needed to facilitate FLASH research and support its clinical translation. Tissue-equivalent scintillators, with millimeter-level spatial resolution and millisecond-level temporal resolution, possess these required characteristics and show strong potential for use in UHDR dosimetry

Purpose: We investigated the performance of the HYPERSCINT RP-FLASH scintillator system at up to 1000 Hz sampling frequency (f_s) for UHDR electron beam dosimetry.

Methods: Four-component calibration and 18 MeV at conventional dose rate (CONV) were used to calibrate the spectral characteristics of the scintillator and its signal-to-dose conversion, respectively. The scintillator was exposed to CONV and UHDR electron irradiation using a LINAC-based FLASH platform. Its dose linearity and dose accuracy in response to the CONV and UHDR irradiation at 1 and 1000 Hz f_s were quantified against ion chamber or EBT-XD film measurements. The response of the scintillator system was investigated as a function of beam energy, field size, dose per pulse (DPP), and pulse repetition frequency (PRF). Relative signal sensitivity was quantified against accumulated dose to account for the scintillator's radiation degradation. Time-resolved UHDR dose per pulse measured by the scintillator were verified using a PMT-fiber optic scattered radiation detector.

Results: The scintillator system demonstrated high dose accuracy, within 0.5% compared to ion chamber measurements, under the CONV electron irradiation at 1 Hz f_s . For the UHDR irradiation, the scintillator showed $<3\%$ dose error compared to film measurement up to 40 Gy at 1000 Hz f_s . We did not observe significant energy dependence for 6 and 18 MeV irradiation, field size dependence ranging from 2×2 to 25×25 cm², DPP dependence from 1 to 2.3 Gy/pulse, and PRF dependence from 30 to 180 Hz. The radiation degradation of the scintillator was quantified using a 2nd-order polynomial, with a linear fit of $-2.6\%/kGy$ for the range of 0 to 2 kGy. The time-resolved dose per pulse measurements at 1000 Hz were verified to be within 3% accuracy when compared to that obtained using the PMT-fiber optic detector.

Conclusions: We conducted a comprehensive investigation into the performance of the HYPERSCINT RP-FLASH scintillator system for electron FLASH research. The system demonstrated good dose linearity and accuracy for both CONV and UHDR electron beams, with minimal dependence on beam energy, field size, DPP, and PRF. Furthermore, it

effectively resolved the temporal characteristics of UHDR beams. These results suggest that the HYPERSCINT RP-FLASH scintillator system could serve as a detector of choice for electron FLASH research.

1. INTRODUCTION

Ultra-high dose rate (≥ 40 Gy/s, UHDR) irradiation has been shown to reduce normal tissue toxicity while maintaining similar tumor control compared to conventional dose rate (~ 0.1 Gy/s, CONV) setting across various animal models and endpoints¹⁻⁴. The differential effect of UHDR between normal tissue and tumor is termed the FLASH effect. The clinical translation of FLASH radiotherapy (RT) has attracted significant interest due to its potential to improve therapeutic ratios, reduce treatment time, and mitigate organ motion-related issues⁴⁻⁶.

The introduction of UHDR radiation presents new dosimetry challenges^{7,8}. Ionization chambers (IC) serve as the clinical reference dosimetry tools for CONV radiation, but most of them exhibit dose rate-dependent ion recombination effects at UHDR⁹. Passive detectors, such as radiochromic film (RCF) and thermoluminescent detector (TLD), show dose rate independence and have been applied to the UHDR measurements^{10,11}. However, these passive detectors require post-irradiation waiting periods, preventing immediate reporting of measurements. In addition to traditional spatial dosimetric measurements like percent depth dose (PDD) and profile, FLASH studies introduce new requirements for resolving beam temporal characteristics. The FLASH effect is observed only above a threshold of average dose rate (ADR)² and may depend on other temporal dosimetry factors such as instantaneous dose rate (IDR), pulse interval, and dose per pulse (DPP)^{12,13}. Therefore, there is a critical need for a detector that is dose rate-independent, fast-responding, and capable of accurately resolving the spatial and temporal characteristics of UHDR beams.

Plastic scintillation detectors (PSDs) have been widely used in CONV because of their favorable dosimetric properties^{14,15}. As fast-responding and water-equivalent dosimeters, PSDs have demonstrated energy independence for clinical electron and photon beams, as well as independence from the angle of incidence in CONV setting^{15,16}. PSDs also offer the advantages of high spatial resolution at the millimeter scale and fast temporal resolution at the order of millisecond¹⁴. Furthermore, their flexibility in design, such as small size, and magnetic field independence make PSDs suitable for small field¹⁷ and MR-LINAC dosimetry¹⁸.

A large portion of FLASH studies including clinical trials have involved electron beams⁴. UHDR electron beams are relatively more accessible than other radiation modalities due to methods developed for converting clinic LIANCs to UHDR mode¹⁹⁻²² and various commercial options²³⁻²⁵. Beyond plastic scintillators' use in CONV RT, efforts have been made to apply them to address electron FLASH dosimetry needs²⁶⁻²⁸. Ashraf et al.²⁶ demonstrated that the Exradin W1 (Standard Imaging, Middleton, WI) responded within 3% of Gafchromic film for

10 MeV UHDR electron beam across dose rates of 40–380 Gy/s, DPP of 0.3–1.3 Gy, and field sizes of 1–4 cm in diameter. Liu et al.²⁷ further characterized the Exradin W2 system with a BCF-12 scintillator, demonstrating mean dose rate independence and linearity as a function of integrated dose and DPP for $\text{DPP} \leq 1.5$ Gy and pulse repetition frequency (PRF) ≤ 90 Hz. Poirier et al.²⁸ investigated the performance of the Hyperscint RP100 plastic scintillator (Medscint, Quebec City, QC, Canada) with a 1 mm diameter x 1 mm length PSD probe under 16 MeV UHDR, reporting readings within 4% of Gafchromic EBT-XD film for 0–40 Gy.

To further advance the knowledge in our field, we conducted a comprehensive evaluation of the HYPERSCINT RP-FLASH scintillation dosimetry system under UHDR electron irradiation. The system is specifically designed for UHDR applications and offers a temporal resolution of up to 1000 Hz. Our study assessed dose linearity and dosimetric accuracy for both CONV (0.1 Gy/s) and UHDR (400 Gy/s) electron beams, alongside the detector's response to key parameters including beam energy (6 and 18 MeV), field size (2x2 to 25x25 cm²), DPP (1 to 2.3 Gy), PRF (30 to 180 Hz), and accumulated dose (up to 10 kGy), covering irradiation conditions typically encountered in electron FLASH studies. These parameters were studied for their potential impact on scintillator performance, with beam energy and field size being factors related to stem effects¹⁵, while DPP, PRF, and accumulated dose were identified as potential limitations to dosimeter performance^{27,29}. Time-resolved measurements of the scintillator at 1000 Hz were validated using a PMT-fiber optic detector, which measures the relative output of electron beam pulses via Cherenkov light generated by scattered radiation in the fiber²⁰.

Our comprehensive study suggests that the HYPERSCINT RP-FLASH scintillator system could be a suitable detector for UHDR electron dosimetry. This work will provide the research community with guidance on utilizing this commercially available scintillator system for electron FLASH research.

2. METHODS

2.1 Configuration and calibration of HYPERSCINT RP-FLASH scintillator system

The HYPERSCINT RP-FLASH system comprises the HYPERSCINT RP-FLASH optical reader (Fig. 1a1), PRB-0042 RP detector (Fig. 1a2-3), and HYPERDOSE software (Version 0.1.15). The HYPERSCINT RP-FLASH optical reader incorporates a spectrometer with an electric cooled 2D photodetector array for light spectrum measurement. The PRB-0042 RP detector is a single channel plastic scintillator probe with a 1 mm diameter x 3 mm length sensitive volume, coupled to a 20 m long polymethyl methacrylate plastic fiber optic. The reader is connected to a computer through USB 3.0 port. The total dose, time-resolved dose distribution at selected sampling frequency (f_s) and measured light spectrum are saved after each measurement. The system functions at f_s 1 to 1000 Hz. If $f_s < 25$ Hz, the system records data continuously until terminated by user. Otherwise, if $25 \text{ Hz} < f_s < 1 \text{ Hz}$, the system records a fixed number of sampling windows with a length of $1/f_s^{30}$. The number of sampling windows is 3000 when $f_s = 1000$ Hz, corresponding to 3s acquisition time.

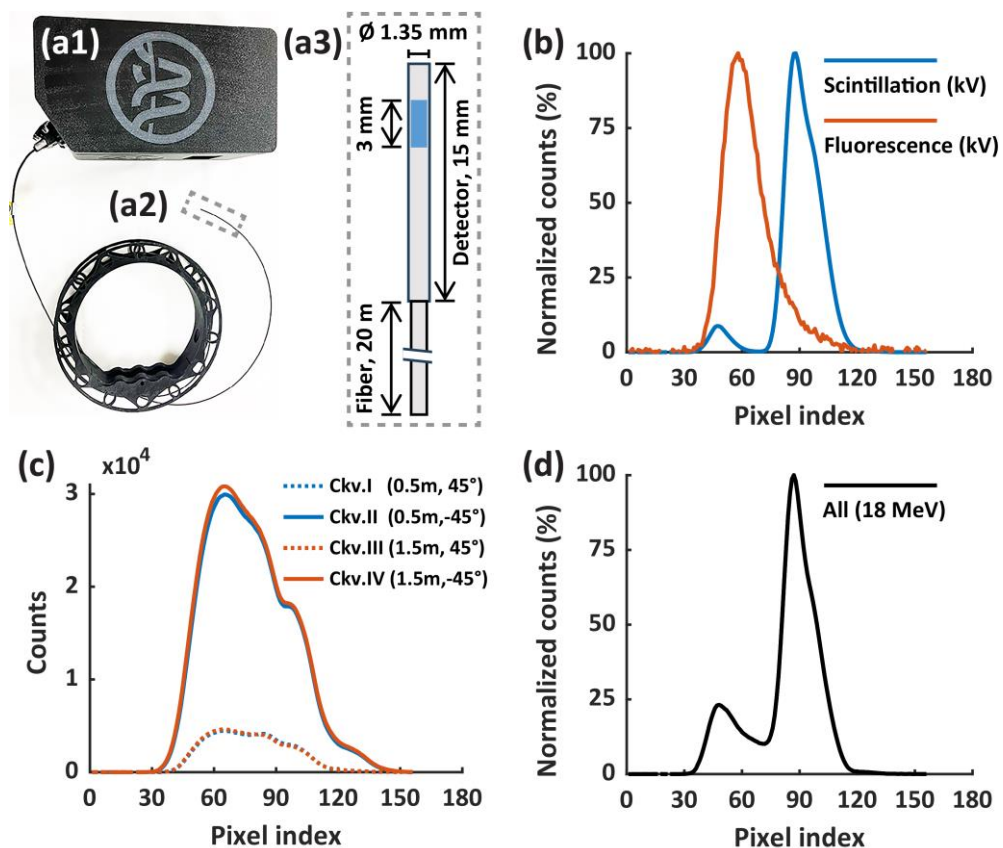


Figure 1. Configuration and calibration of the HYPERSCINT RP-FLASH scintillation dosimetry system. The HYPERSCINT RP-FLASH system comprises (a1) HYPERSCINT RP-FLASH optical reader, (a2) PRB-0042 RP detector, and HYPERDOSE software (not shown). (a3) illustrates the PRB-0042 RP dimension, sensitive volume (blue square, 1 mm diameter x 3 mm length) and optical fiber.

(b) shows the spectrum of scintillation and fluorescence introduced by kV X-ray source. (c) shows the spectrum of Cherenkov I&II (irradiated at 0.5 m from probe tip, $\pm 45^\circ$ gantry angle) and Cherenkov III&IV (irradiated at 1.5 m from probe tip, $\pm 45^\circ$ gantry angle) introduced by 6 MV source. (d) is the spectrum after dose calibration using 18 MeV. Abbreviations: Ckv.I-IV, Cherenkov I-IV.

The interaction of scintillator material with radiation results in the emission of optical photons, termed scintillation, and the number of scintillation photons is proportional to the absorbed dose. However, Cherenkov and fluorescence photons produced within both the scintillator and fiber optic would contaminate the scintillation signal, as they are not dose-proportional but related to other factors, such as the length of fiber optics irradiated. In the HYPERSCINT RP-FLASH system, the measured light signal is assumed to be a linear superposition of scintillation, fluorescence and Cherenkov photons. A hyperspectral approach was adopted to decompose the light components and calculate the dose with improved precision and robustness compared to other methods^{31,32}. Dose and spectral calibrations are thus necessary for the hyperspectral approach.

The dose calibration was performed in an electron FLASH LINAC³³, which was converted from a Clinac 21EX LINAC (Varian 21EX, Varian Medical Systems, Palo Alto, CA). Due to the absence of kV sources in the 21EX LINAC, the spectral calibration was conducted in a TrueBeam LINAC (Varian TrueBeam, Varian Medical Systems, Palo Alto, CA). Following the vendor recommendation, 4-component calibration was used for the spectral calibration, consisting of scintillation, fluorescence, Cherenkov I&II and Cherenkov III&IV. The scintillation component was acquired by irradiating the probe tip with minimal length of fiber optic by the kV imager of the TrueBeam, while the fluorescence component was characterized by irradiating 10 loops of the fiber optic while sparing the sensitive volume. The nominal energy of the kV beam is 90 kVp, lower than the Cherenkov light production energy threshold in the fiber optic. Figure 1b shows the scintillation and fluorescence spectrum measured by the HYPERSCINT system. Cherenkov I&II were acquired by irradiating the fiber optic at 0.5m from the probe tip by 6 MV of the TrueBeam, with a 45° or -45° gantry angle, 100 cm source-to-surface distance (SSD), open field and 6 cm solid water backscatter. All the setups were the same for Cherenkov III&IV, except at 1.5m from the probe tip. Figure 1c shows the spectrum of Cherenkov I&II and Cherenkov III&IV. The rationale to irradiate different locations of the fiber with various angles is to account for light attenuation in fiber optic and the directivity of Cherenkov light. Dose calibration was performed by delivering 500 monitor unit (MU) of 18 MeV CONV from the Clinac 21EX at 100 cm SSD, with a 10×10 cm² cone, at 2 cm depth, established by 1 cm solid water and 1 cm bolus, with 6 cm solid water as the backscatter piece.

The probe tip was aligned to the crosshair of LINAC. Because of the flat depth dose features around 2 cm of 18 MeV CONV and its energy close to the 18 MeV UHDR beam used in our FLASH animal studies, we chose the 18 MeV CONV for dose calibration. The 18 MeV CONV dose delivered to the scintillator probe was quantified by output measurement with an ADLC-calibrated Semiflex 31013 IC (PTW-Freiburg, Freiburg, Germany) at 2 cm depth. Figure 1d is the normalized light spectrum resulting from the 18 MeV CONV irradiation. The detector remained connected to the reader throughout the entire study to avoid potential calibration spectrum mismatch after unplugging and re-plugging the detector²⁸. Dose calibration was performed prior to measurements to ensure accuracy.

2.2 Film dosimetry

Gafchromic EBT-XD films (Ashland, Bridgewater, NJ) were used to validate the scintillator's UHDR measurements, as the films have demonstrated dose rate independence at UHDR^{7,34}. The films were scanned 24 hours post-irradiation using a flatbed photo scanner (Epson Expression 12000XL, Nagano, Japan). An in-house film analysis software was employed to extract dose information from the films, utilizing a two-channel method (green and blue)³⁵. The average readings in the central 5x5 mm² of films were used for the dosimetric analysis. The film dosimetry was also validated against IC measurements in CONV within 3% for the dose ranging from 0 to 40 Gy.

2.3 CONV and UHDR measurements

Unless otherwise stated, all CONV and UHDR measurements were performed using the Clinac 21EX at 100 cm SSD, with a 10x10 cm² cone, at 2 cm depth, and 6 cm of solid water for backscatter (Fig. S1a), consistent with the calibration setup (Sec. 2.1). The scintillator probe tip was aligned with the crosshair. The above setup is referred to as the standard setup. For UHDR measurements, a piece of film was directly placed beneath the scintillator probe (Fig. S1b). The radiation and study parameters of CONV and UHDR irradiation are summarized in Table S1. Later, in Sec. 3.2, we show that there is no energy dependence on the detector response. Moreover, our animal FLASH experiment is conducted by 18 MeV FLASH, which provides superior dose homogeneity than lower energy electron beam. We therefore chose the 18 MeV beam as the default modality throughout this study.

Unless otherwise stated, all measurements reported in this study represent the average of 3 consecutive measurements, with error bars indicating the standard deviation of these measurements. The error bar for ratio analysis, such as the one in Fig. 2a2, represents its standard deviation calculated through propagation of uncertainty:

$$\frac{\sigma_c}{c} = \left[\left(\frac{\sigma_a}{a} \right)^2 + \left(\frac{\sigma_b}{b} \right)^2 \right]^{\frac{1}{2}} \quad (1)$$

where $c = a/b$, σ_a , σ_b and σ_c are the standard deviations of a , b and c , respectively. Note that the error bars may not be visible if they are smaller than the symbols representing the average values.

2.4 Dose linearity and dosimetric accuracy in measuring CONV and UHDR electron beams

The dose linearity and dosimetric accuracy of the scintillator system were quantified under both 18 MeV CONV and UHDR electron irradiation. For 18 MeV CONV, 1–3500 MU were delivered and the dose to the scintillator was quantified by the ADLC-calibrated Semiflex 31013 IC. Due to the long delivery time of CONV, 1 Hz sampling frequency was used. For 18 MeV FLASH, 2–17 pulses were delivered at both 1 and 1000 Hz. The dose delivered under the UHDR were verified against film measurements.

2.5 Beam energy dependence of the scintillator under CONV

Given the water equivalence of PSDs, there should not be any energy dependence of the scintillator system for clinical electron and photon beams. However, the intensity of Cherenkov and fluorescence light induced in the fiber depends on the beam energy³⁶, influencing the hyperspectral method used to decompose light signals. The system's energy dependence was studied under CONV irradiation rather than UHDR and the reasons were twofold: first, IC measurements for CONV-RT provide less dosimetric uncertainties compared to film measurements for UHDR; second, our results (Sec. 3.1) indicate that the system exhibits no dose rate dependence between 0.1 and 400 Gy/s in terms of dosimetric linearity and accuracy. Therefore, 6 and 18 MeV at CONV were adopted to assess the scintillator's energy response. The dose outputs of the 6 and 18 MeV CONV were quantified by IC and then compared with the scintillator measurements.

2.6 Field size dependence

Field size determines the length of fiber optics irradiated, thereby affecting the amount of fluorescence and Cherenkov light produced, a phenomenon known as the stem effect¹⁵. We quantify if the scintillator responses as a function of field size by comparing the field size factor (f_{FS}) measured by the scintillator with that measured by the IC. The f_{FS} was defined as the dosimetric reading measured at a 2 cm depth with a specific field size, relative to that measured with a 10x10 cm² field. For both 6 and 18 MeV CONV beams, f_{FS} for 6x6 to 25x25 cm²

measured by the scintillator and IC (PTW Semiflex 31013) were compared. The chamber measurements were also verified with Varian golden beam data, showing a difference within 1% (Fig. S2). Additionally, the f_{FS} of the smaller field sizes 2x2 and 4x4 cm² were compared between scintillator and CC13 ion chamber (3 mm radius x 5.8 mm length cavity, IBA dosimetry, Schwarzenbruck, Germany).

2.7 Dose per pulse (DPP) dependence

To investigate the DPP dependence of the scintillator system for UHDR electron irradiation, ten 18 MeV UHDR pulses were delivered at various SSD setups (100–140 cm), resulting in 1 to 2.3 Gy DPP. All the other setups were consistent with the default setting at 1000 Hz (Table S1). The DPP was determined by the effective SSD method (see supplementary material Sec. 4).

2.8 Pulse repetition frequency (PRF) dependence

We examined if the system's response depends on the PRF in the range from 30 to 180 Hz by delivering 4 to 17 pulses to the scintillator, with a DPP of 2.3 Gy. The PRF was adjusted by setting the repetition rate from 100 to 600 MU/min in the LINAC console, with the maximum PRF of 180 Hz for 18 MeV UHDR. The PRFs of the delivered beams were verified by a remote trigger unit (RTU; DoseOptics, Lebanon, NH) positioned outside the radiation field (Fig. S4). The RTU is a coincidence-based radiation detector; it consists of two scintillators and corresponding silicon photomultipliers (SiPMs) to detect scattered radiation³⁷.

2.9 Radiation degradation

To quantify the radiation degradation of the scintillator and fiber optic, the detector degradation factor (DDF) was evaluated as a function of the accumulated dose:

$$DDF(D_a) = \frac{Rdg(D_a)}{Rdg(D_0)} \quad (2)$$

where D_a is the accumulated dose, defined as the dose delivered to the scintillator without dose recalibration performed. $Rdg(D_a)$ represents the scintillator's reading after measuring 100 MU of 18 MeV CONV using the standard setup at D_a . On the other hand, $Rdg(D_0)$ is the scintillator's reading under the same condition acquired immediately after calibration, when the radiation-induced degradation affecting the scintillator reading is eliminated.

A total D_a of around 10 kGy was delivered to the scintillator within 2 hours using 18 MeV UHDR. Since the scintillator's reading may be subject to uncertainty due to the radiation degradation, an independent detector is required to determine D_a delivered to the scintillator.

A CC13 IC was placed under the edge of the electron cone (Fig. S5a) to measure the Bremsstrahlung and scattered radiation. Due to the relatively small sensitive volume of CC13 (0.13 cm^3) and the low dose rate of Bremsstrahlung and scattered radiation, the CC13 reading has been shown to be linear with the FLASH dose delivered to the scintillator (Fig. S5b). The accumulated dose D_a to the scintillator can thus be quantified based on the CC13 reading.

2.10 Verification of temporal dosimetric measurements

To verify the time-resolved measurements of the scintillator system, the measured pulse structure was compared against a pulse form monitoring unit. The unit consists of an HC-120 series photomultiplier tube (PMT; Hamamatsu, Shizuoka, Japan) coupled with an optical fiber, enabling the detection of scattered radiation through radiation-induced Cherenkov emission²⁰. The PMT output was fed into an oscilloscope (70MHz, PicoScope 3000 series, Pico Technology, Cambridgeshire, UK), allowing us to monitor the LINAC pulse amplitudes on a pulse-by-pulse basis. The normalized area under curve (AUC) of the pulse form was then compared to the normalized DPP measured by the scintillator. Ten measurements were performed for both the scintillator and PMT to account for the uncertainties of PMT measurements, which arise from the stochastic nature of scattered radiation.

3. RESULTS

3.1 Dose linearity and dosimetric accuracy in measuring CONV and UHDR electron irradiation

The performance of the scintillator in response to 18 MeV CONV and UHDR was benchmarked against IC and film measurements, respectively. As shown in Fig. 2a1, the scintillator at 1 Hz demonstrated good linearity compared to IC measurements for 18 MeV CONV up to 35 Gy. The scintillator achieved accuracy $< 0.5\%$ difference compared to the IC measurements from 0.1 to 35 Gy, and larger deviation is seen for dose < 0.1 Gy (Fig. 2a2).

For 18 MeV UHDR, Fig. 2b1 shows that the scintillator at 1 Hz displayed reasonable linearity up to ~ 18 Gy, but saturation was observed after 18 Gy, which was consistent with the spectrum measured after 4 pulses (9 Gy) and 17 pulses (40 Gy) delivered (Fig. 2b2). It renders that the non-linear response observed at 1 Hz likely resulted from large amount of light signal collected within a sampling window exceeding the dynamic range of the photodetector array during UHDR irradiation. While we increased the sampling frequency to 1000 Hz, we can resolve the saturation issue. Compared to the film measurements, the scintillator at 1000 Hz showed good dose linearity ($R^2 > 0.999$) and within 3% accuracy up to 40 Gy (Fig. 2c1-2).

3.2 Beam energy dependence of the scintillator under CONV irradiation

As shown in Table S2, the relative differences between the scintillator and IC measurements after 100 MU of 6 MeV and 18 MeV CONV irradiation were $1.81 \pm 2.18\%$ and $0.18 \pm 0.13\%$, respectively, which is not statistically significant different ($p = 0.325$). These results indicate that there is no obvious energy dependence of the scintillator between 6 and 18 MeV.

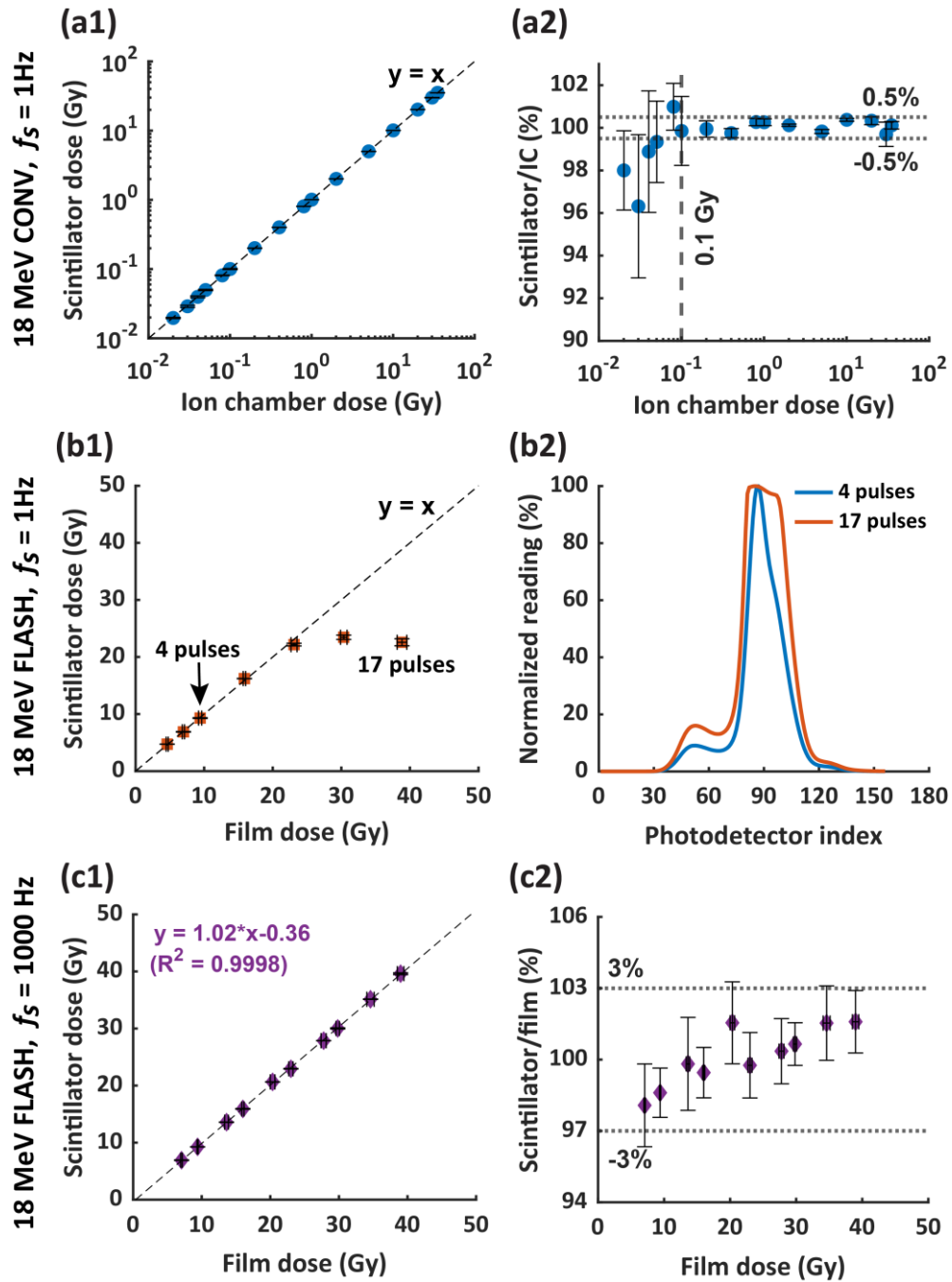


Figure 2. Dose linearity and accuracy of the scintillator under CONV and UHDR electron irradiation at different sampling frequencies. (a1-2) show the readings of the scintillator at 1 Hz compared to IC measurements and the ratio of the measurements under 18 MeV CONV. (b1) shows the readings of the scintillator at a 1 Hz against EBT-XD film under 18 MeV UHDR; (b2) is the corresponding light spectrum measured by the scintillator after receiving 4 and 17 pulses of 18 MeV UHDR. (c1-2) show the dose measured by scintillator at 1000 Hz compared to that of film and their ratio under 18 MeV UHDR. Abbreviations: f_s , sampling frequency; CONV, conventional dose rate; UHDR, ultra-high dose rate; IC, ionization chamber.

3.3 Field size dependence

Figure 3a shows the field size factors f_{FS} of 6 and 18 MeV CONV measured by the scintillator and IC from 2x2 to 25x25 cm². In contrast to 18 MeV, f_{FS} of 6 MeV rapidly increased from 2x2 to 4x4 cm² and reached saturation, partly due to the sharp drop of the depth dose at the 2 cm depth of measurement for the 2x2 cm² field. Figure 3b illustrates the ratio of f_{FS} measured by the scintillator to those measured by the IC. The scintillator and IC measurements agreed within 1.5% accuracy, indicating that the scintillator exhibits <1.5% field size dependence from 2x2 to 25x25 cm² for both energies.

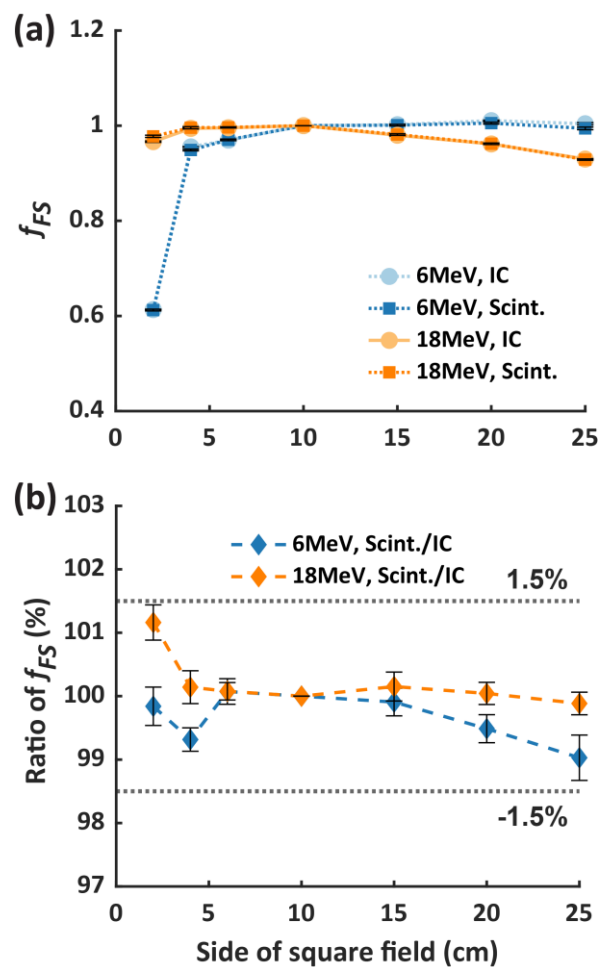


Figure 3. Filed size dependence of the scintillator under 6 and 18 MeV UHDR irradiation. (a) shows the field size factor f_{FS} measured by the scintillator and IC, and (b) is the corresponding f_{FS} ratio. Abbreviations: f_{FS} , field size factor; IC, ion chamber; Scint., scintillator.

3.4 Dose per pulse (DPP) dependence of the scintillator

Figure 4a shows the readings of the scintillator after receiving 10 pulses of 18 MeV at UHDR with respect to DPP ranging from 1 to 2.3 Gy. The readings were normalized at 2.3 Gy DPP. The $R^2 > 0.999$ renders good linearity of scintillator measurement for a given DPP. Figure 4b further shows the ratio of the scintillator-measured dose to the expected dose for a given DPP after 10 pulses delivered. We observed $< 3\%$ between the scintillator and expected dose over the range of 1–2.3 Gy DPP, indicating minimum DPP dependence observed.

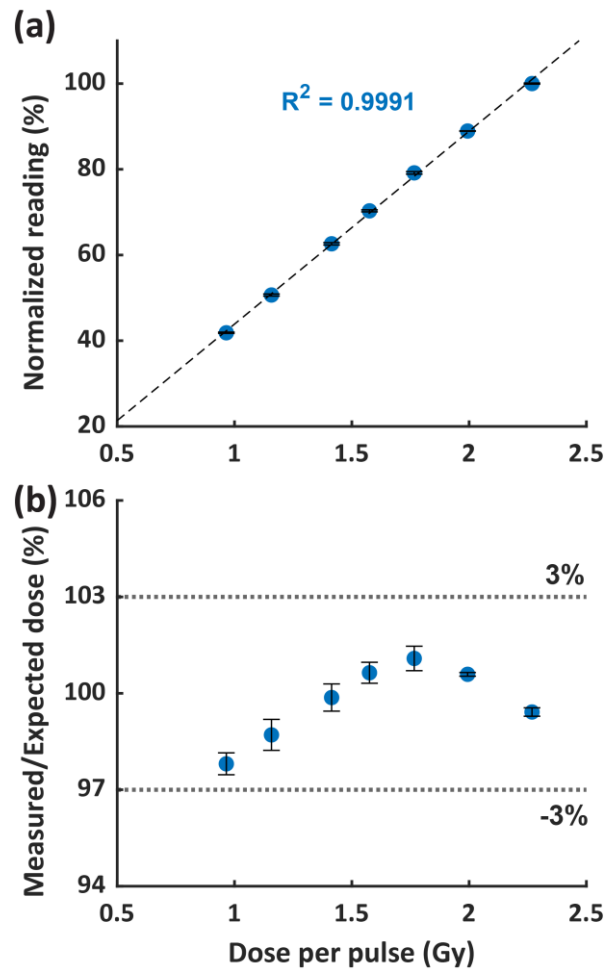


Figure 4. Dose per pulse dependence of the scintillator under 18 MeV UHDR irradiation. (a) shows the normalized scintillator reading after ten 18 MeV UHDR pulses delivered with respect to DPP, normalized to the reading at 2.3 Gy per pulse. (b) is the ratio of the scintillator-measured dose to the expected dose vs DPP.

3.5 Pulse repetition frequency (PRF) dependence

We analyzed the impact of PRF on scintillator measurements by delivering 4 to 17 pulses of 18 MeV at UHDR, with PRF ranging from 30 to 180 Hz (Fig. 5). For the 4 pulses scenario, with 9 Gy delivered, minimum PRF dependence (within 1%) was observed. For 10 to 17 pulses, 23-40 Gy delivered, the normalized readings decreased as the PRF increased, though the variation among PRF settings was less than 2%.

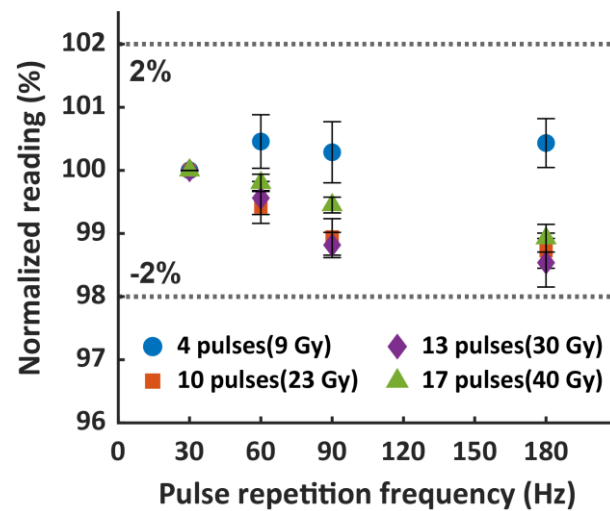


Figure 5. Normalized scintillator reading versus 30–180 Hz PRF after receiving 4–17 pulses of 18 MeV at UHDR (9–40 Gy).

3.6 Radiation degradation

Figure 6a shows the detector degradation factor (DDF, see Sec. 2.9) as a function of the accumulated dose. The DDF can be modeled by a 2nd-order polynomial fit up to 10 kGy. We provide a quick estimation of 2.65%/kGy degradation after 2 kGy delivered to scintillator, which can serve as a guide for dose recalibration. Figure 6b illustrates the measured light spectrum with respect to the accumulated dose. Detector degradation was observed to result not only in a reduction of the scintillator signal but also in changes to the light spectrum, as evidenced by the diminishing small peak at a photodetector index of approximately 45 with increasing accumulated dose.

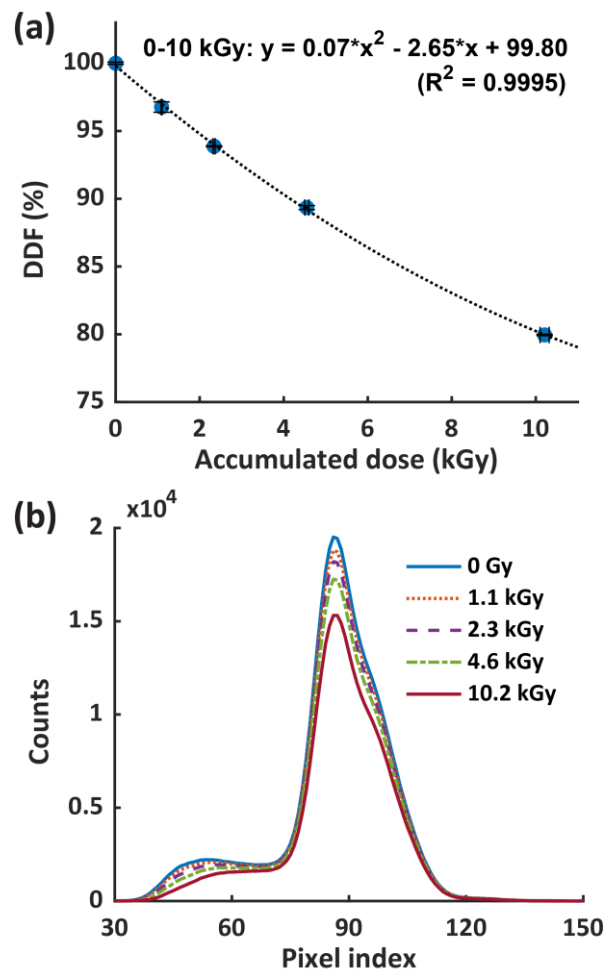


Figure 6. (a) is DDF of the scintillator and (b) is the associated light spectrum with respect to the accumulated dose. Abbreviation: DDF, detector degradation factor.

3.6 Verification of time-resolved dosimetric measurement

The PMT-fiber optic detector is able to measure an individual pulse (Fig. 7a). Figure 7b shows the normalized pulse-resolved readings of the scintillator and PMT after 10 pulses of 18 MeV UHDR irradiation. The reading of the scintillator refers to the measured dose per pulse, while the reading of the PMT represented the AUC of the detected signal in response to each pulse (Fig. 7a). The pulse resolved readings from both detectors were normalized to each detector's average reading of the 10 pulses, respectively. The scintillator and PMT readings both showed a consistent lower amplitude for the 1st pulse and a higher amplitude for the 2nd one, while for the remaining pulses, the results were relatively stable. Figure 7c further illustrates that the ratio between the scintillator and PMT readings agrees within 3%. A large standard deviation of the ratio is observed due to the uncertainty of the PMT signal, which stems from the stochastic nature of the scattered radiation. This result verified the capability of the scintillator in resolving single pulse during UHDR electron irradiation.

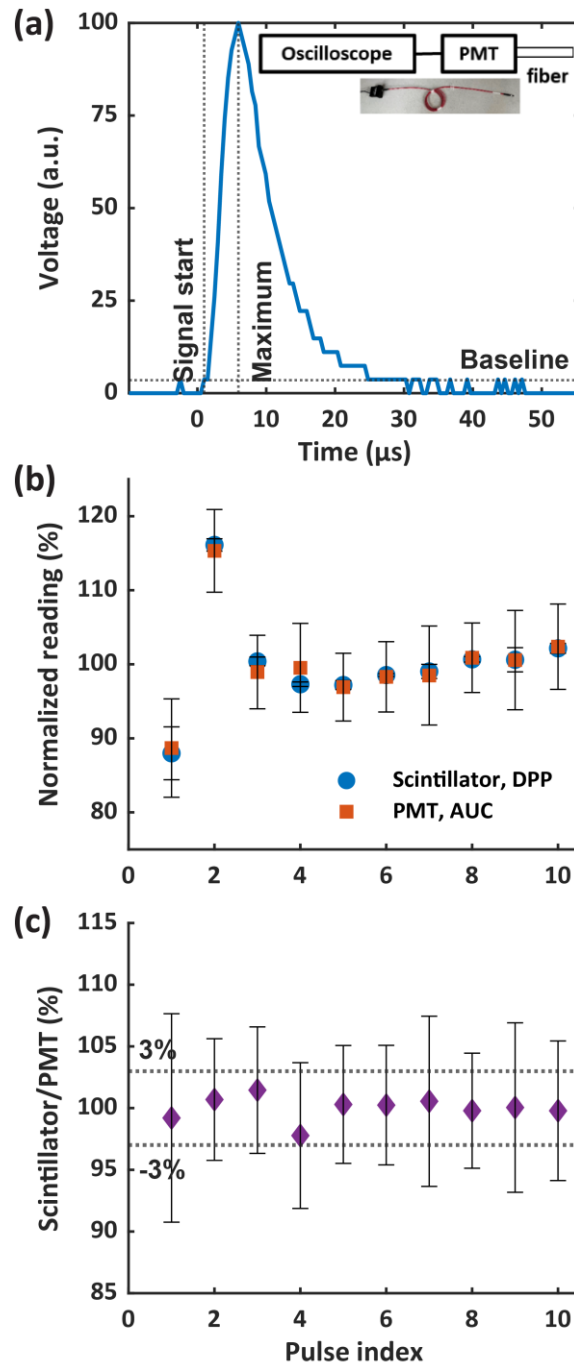


Figure 7. Comparison of the scintillator and PMT measurements for a given pulse structure. (a) shows the configuration of the scattered radiation-based pulse form monitoring unit, which consists of a PMT coupled with an optical fiber, and its pulse form after receiving one 18 MeV UHDR pulse. (b) shows the comparison of the relative pulse-resolved reading of the scintillator (DPP) and PMT (AUC) after ten 18 MeV UHDR pulses, normalized to the average reading of the 10 pulses. (c) shows the corresponding ratio of the scintillator and PMT measurements. Abbreviations: AUC, area under curve; DPP, dose per pulse; PMT, photomultiplier tube.

4. DISCUSSION

FLASH-RT has sparked tremendous interest in the radiation oncology community. However, the introduction of UHDR radiation presents substantial dosimetric challenges, particularly in accurately measuring radiation dose under conditions of high dose per pulse within an extremely short period of time, i.e. high instantaneous dose rate. Accurate, dose rate independent, fast-response, and time-resolved dosimeters are therefore essential for FLASH studies. Scintillators have emerged as detectors of choice to address these challenges^{26-28,30,34,38-40}. Our study provides a comprehensive characterization of the HYPERSCINT RP-FLASH scintillator, demonstrating its suitability as a dosimeter for UHDR electron research.

The HYPERSCINT RP-FLASH scintillator system exhibited high accuracy in dose measurements for both CONV (~0.1 Gy/s) and UHDR (400 Gy/s) electron irradiation (Fig. 2). With accuracy within 0.5% over the dose range of 0.1 to 35 Gy in CONV mode, the system aligns with the performance of previous HYPERSCINT versions at extended dose ranges^{41,42}. However, nonlinear behavior in scintillator response was observed at the 1 Hz sampling frequency when doses <0.1 Gy or >18 Gy were delivered. These nonlinearities are likely due to the photodetector's signal processing limitations: at low doses, measurement accuracy is compromised by system noise perturbing the weak light signal, while at high doses, the light signal exceeds the detector's dynamic range (Fig. 2b2). Increasing the frequency, which shortens the sampling window and reduces the dose measured per window, effectively mitigates the saturation effect observed at higher doses. At the 1000 Hz sampling frequency, the scintillator achieved <3% dose variation compared to the film measurements up to 40 Gy, covering the dose range used in most FLASH studies. Since direct reference dosimetry for UHDR electron beams traceable to metrological standards is currently unavailable, EBT-XD film, with a dose accuracy of ~ 3%, was used as a substitute. The precision of the film in dose measurement thus limits the upper bound of our assessment of scintillator performance. We expect the actual accuracy of the RP-FLASH scintillator in UHDR dosimetric measurement to be better than 3%.

The stem effect poses a challenge in scintillator dosimetry, as it can introduce errors in dose measurements¹⁵. Beam energy is one factor influencing the stem effect. While the scintillation signal of plastic scintillators is independent of incident particle's energy above ~125 keV¹⁵, the intensity of Cherenkov and fluorescence light induced in the fiber depends on the beam energy³⁶. The RP-FLASH scintillator demonstrated < 2% dependence between 6 and 18 MeV (Table S2), suggesting that variations in Cherenkov and fluorescence intensity with beam

energy are effectively accounted for. Additionally, field size can influence the stem effect by determining the volume of fiber irradiated and, consequently, the intensity of Cherenkov and fluorescence light. Beierholm et al.⁴³ reported that the ratio of output factors measured by Exradin W1 system and IC are up to 3.3% for fields of 2x2–10x10 cm² and remain within ~0.8% for larger fields 10x10–25x25 cm² at 6–15 MV. In comparison, the HYPERSCINT RP-FLASH scintillator showed <1.5% deviation across 2x2 to 25x25 cm² for 6 and 18 MeV (Fig. 3b). These results suggest that the hyperspectral method effectively mitigates the stem effect by addressing variations in Cherenkov and fluorescence light intensity as a function of beam energy and field size, ensuring high accuracy in UHDR dosimetry.

Dose per pulse is a known limiting factor for the performance of scintillators. Since tuning pulse width is not feasible with our electron FLASH platform, we modified DPP by varying SSD and concurrently instantaneous dose rate to assess its effect on scintillator performance. This method has been used in previous studies^{27,30} to evaluate the DPP dependence of PSDs. Liu et al.²⁷ observed that the Exradin W2 scintillator saturates at DPPs exceeding 1.5 Gy. Baikalov et al.³⁰ reported within 2% signal decrease for the same RP-FLASH scintillator as this study at 0.4–2.2 Gy DPP and a 2–6% decrease for 2.2–7.7 Gy. Our findings of within 3% dependence results for the range of 1–2.3 Gy DPP (Fig. 4) are slightly higher than their observation. Adjusting SSD with the same electron cone inherently alters the field size. In this study, SSDs of 100–140 cm corresponds to field sizes of 10x10–14x14 cm² defined at surface. From Fig. 3b, the scintillator only exhibited <0.2% variation between 10x10–14x14 cm², suggesting that field size would not play significant factor to the observed DPP dependence of the RP-FLASH scintillator (Fig. 4b).

Pulse repetition frequency may influence scintillator performance in UHDR dosimetry, particularly at high DPP levels. Liu et al.²⁷ observed a ~11% and ~0.5% reduction in the blue and green channel signals of the W2 scintillator at 120 Hz compared to 10 Hz at a DPP of 2.34 Gy. They hypothesized that this dependence was due to limitations in the electrometer's signal processing capabilities. In contrast, the HYPERSCINT system, which uses a photodetector array instead of an electrometer as the readout unit, exhibited < 2% dependence on PRF between 30 and 180 Hz at a comparable DPP of 2.3 Gy (Fig. 5). These findings highlight the potential of the HYPERSCINT system to mitigate PRF-related signal variation in PSDs for UHDR dosimetry.

Plastic scintillators have demonstrated both permanent and temporal signal degradation due to radiation exposures⁴⁴. The signal recovery due to the temporal degradation can occur over approximately two months⁴⁵. Notably, higher dose rates irradiation introduces less permanent

damage to the scintillator thus more temporal degradation⁴⁴. Recent studies have examined the radiation damage to plastic scintillators used in UHDR dosimetry^{26,27,30}, with findings ranging from no evident signal degradation to 16%/kGy. However, the dose rates in these studies were not reported explicitly, complicating the interpretation of results. Recently, Giguère et al.⁴⁵ delivered 37.2 kGy of 200 MeV very high energy electron beam at fixed ~ 40 Gy/s to the Medscint scintillator and reported a 1.55%/kGy light output loss. In our study, ~ 10 kGy of 18 MeV electrons were delivered at ~ 400 Gy/s over a period of 2 hours shorter than the reported 2 months recovery period⁴⁵. We observed a decrease in the DDF that followed a 2nd-order polynomial trend, with a linearly fitted degradation rate of 2.65%/kGy for 0–2 kGy (Fig. 6a). The difference between the degradation rates of 1.55%/kGy and 2.65%/kGy likely arises from the dose rate difference (~ 40 Gy/s vs. ~ 400 Gy/s), which may have difference in the temporal damage. A smaller degradation rate and DDF are expected for the RP-FLASH scintillator after the detector resolved from the temporal damage. Additionally, we demonstrated that radiation degradation of the scintillator is associated with both signal reduction and changes in the scintillator's light spectrum (Fig. 6b), consistent with the findings of Giguère et al.⁴⁵. Based on our findings, we recommend a conservative practice; performing dose recalibrations daily and whenever the accumulated dose reaches 2 kGy to ensure dose measurement accuracy within 3%.

In addition to the average dose rate, temporal characteristics of the FLASH beam, such as dose per pulse, have been shown to influence the FLASH effect¹³, emphasizing the need for a time-resolved UHDR dosimeter. Beam current transformer⁴⁶ and PMT-fiber optic detectors²⁰ can measure time-resolved dosimetric parameters with high temporal resolution, but in a relative manner. Previous studies have shown that scintillators are capable of reporting absolute time-resolved dose measurements^{26,28}, however no verification was provided. In this study, we verified the accuracy of RP-FLASH scintillator for resolving individual pulse against the PMT-fiber optic measurements within 3% deviation. This result demonstrates that the scintillator system can perform pulse counting, quantify dose per pulse, and determine instantaneous dose rate provided known pulse width.

5. CONCLUSIONS

This study comprehensively investigated the performance of the HYPERSCINT RP-FLASH scintillator system for electron UHDR research. The scintillator system demonstrated good dose linearity and accuracy for both CONV and UHDR electron beams, with minimal dependence on beam energy (6 and 18 MeV), field size (2×2 – 25×25 cm²), dose per pulse (1–

2.3 Gy), and pulse repetition frequency (30–180 Hz). The signal sensitivity degradation followed a 2nd-order polynomial fitting, with -2.6%/kGy for 0–2 kGy. The system was also capable of resolving the temporal characteristics of UHDR beams with a 1000 Hz temporal resolution. Our study suggests that the HYPERSCINT RP-FLASH scintillator system could be a suitable detector for UHDR electron research.

ACKNOWLEDGEMENTS

The authors acknowledge the funding support from Cancer Prevention and Research Institute of Texas, RR200042. They also thank François Therriault-Proulx, Benjamin Côté and Danahé LeBlanc (MedScint, Quebec City, Canada) for technical support and useful discussion.

CONFLICTS OF INTEREST STATEMENT

The authors have no relevant conflicts of interest to disclose.

DATA AVAILABILITY STATEMENT

Data are available from the corresponding authors upon reasonable request.

REFERENCES

1. Favaudon V, Caplier L, Monceau V, et al. Ultrahigh dose-rate FLASH irradiation increases the differential response between normal and tumor tissue in mice. *Sci Transl Med.* 2014;6(245):245ra293. <https://doi.org/10.1126/scitranslmed.3008973>
2. Montay-Gruel P, Petersson K, Jaccard M, et al. Irradiation in a flash: Unique sparing of memory in mice after whole brain irradiation with dose rates above 100Gy/s. *Radiother Oncol.* 2017;124(3):365-369. <https://doi.org/10.1016/j.radonc.2017.05.003>
3. Vozenin MC, De Fornel P, Petersson K, et al. The advantage of FLASH radiotherapy confirmed in mini-pig and cat-cancer patients. *Clin Cancer Res.* 2019;25(1):35-42. <https://doi.org/10.1158/1078-0432.CCR-17-3375>
4. Vozenin MC, Bourhis J, Durante M. Towards clinical translation of FLASH radiotherapy. *Nat Rev Clin Oncol.* 2022;19(12):791-803. <https://doi.org/10.1038/s41571-022-00697-z>
5. Bourhis J, Montay-Gruel P, Gonçalves Jorge P, et al. Clinical translation of FLASH radiotherapy: Why and how? *Radiother Oncol.* 2019;139:11-17. <https://doi.org/10.1016/j.radonc.2019.04.008>
6. Bourhis J, Jeanneret Sozzi W, Gonçalves Jorge P, et al. Treatment of a first patient with FLASH-radiotherapy. *Radiother Oncol.* 2019;139:18-22. <https://doi.org/10.1016/j.radonc.2019.06.019>
7. Romano F, Bailat C, Gonçalves Jorge P, Franz Lerch ML, Darafsheh A. Ultra-high dose rate dosimetry: Challenges and opportunities for FLASH radiation therapy. *Med Phys.* 2022;49(7):4912-4932. <https://doi.org/10.1002/mp.15649>
8. Esplen N, Mendonca MS, Bazalova-Carter M. Physics and biology of ultrahigh dose-rate (FLASH) radiotherapy: a topical review. *Phys Med Biol.* 2020;65(23):23TR03. <https://doi.org/10.1088/1361-6560/abaa28>
9. Gonçalves Jorge P, Jaccard M, Petersson K, et al. Dosimetric and preparation procedures for irradiating biological models with pulsed electron beam at ultra-high dose-rate. *Radiother Oncol.* 2019;139:34-39. <https://doi.org/10.1016/j.radonc.2019.05.004>
10. Rahman M, Ashraf MR, Gladstone DJ, et al. Treatment planning system for electron FLASH radiation therapy: open-source for clinical implementation. *Int J Radiat Oncol Biol Phys.* 2022;112(4):1023-1032. <https://doi.org/10.1016/j.ijrobp.2021.10.148>

11. Miles D, Sforza D, Wong J, Rezaee M. Dosimetric characterization of a rotating anode x-ray tube for FLASH radiotherapy research. *Med Phys*. 2024;51(2):1474-1483. <https://doi.org/10.1002/mp.16609>
12. Vozenin MC, Montay-Gruel P, Limoli C, Germond JF. All irradiations that are ultra-high dose rate may not be FLASH: The critical importance of beam parameter characterization and in vivo validation of the FLASH effect. *Radiat Res*. 2020;194(6):571-572. <https://doi.org/10.1667/RADE-20-00141.1>
13. Liu K, Waldrop T, Aguilar E, et al. Redefining FLASH radiation therapy: The impact of mean dose rate and dose per pulse in the gastrointestinal tract. *Int J Radiat Oncol Biol Phys*. 2024. <https://doi.org/10.1016/j.ijrobp.2024.10.009>
14. Beddar AS. Plastic scintillation dosimetry and its application to radiotherapy. *Radiat Meas*. 2006;41:S124-S133. <https://doi.org/10.1016/j.radmeas.2007.01.002>
15. Beaulieu L, Beddar S. Review of plastic and liquid scintillation dosimetry for photon, electron, and proton therapy. *Phys Med Biol*. 2016;61(20):R305-R343. <https://doi.org/10.1088/0031-9155/61/20/R305>
16. Beddar AS, Mackie TR, Attix FH. Water-equivalent plastic scintillation detectors for high-energy beam dosimetry: II. Properties and measurements. *Phys Med Biol*. 1992;37(10):1901. <https://doi.org/10.1088/0031-9155/37/10/007>
17. Létourneau D, Pouliot J, Roy R. Miniature scintillating detector for small field radiation therapy. *Med Phys*. 1999;26(12):2555-2561. <https://doi.org/10.1118/1.598793>
18. Ferrer C, Huertas C, García D, Sáez M. Dosimetric characterization of a novel commercial plastic scintillation detector with an MR-Linac. *Med Phys*. 2023;50(4):2525-2539. <https://doi.org/10.1002/mp.16204>
19. Schüller E, Trovati S, King G, et al. Experimental platform for ultra-high dose rate FLASH irradiation of small animals using a clinical linear accelerator. *Int J Radiat Oncol Biol Phys*. 2017;97(1):195-203. <https://doi.org/10.1016/j.ijrobp.2016.09.018>
20. Rahman M, Ashraf MR, Zhang R, et al. Electron FLASH delivery at treatment room isocenter for efficient reversible conversion of a clinical LINAC. *Int J Radiat Oncol Biol Phys*. 2021;110(3):872-882. <https://doi.org/10.1016/j.ijrobp.2021.01.011>
21. Lempart M, Blad B, Adrian G, et al. Modifying a clinical linear accelerator for delivery of ultra-high dose rate irradiation. *Radiother Oncol*. 2019;139:40-45. <https://doi.org/10.1016/j.radonc.2019.01.031>

22. Xie DH, Li YC, Ma S, et al. Electron ultra-high dose rate FLASH irradiation study using a clinical linac: Linac modification, dosimetry, and radiobiological outcome. *Med Phys*. 2022;49(10):6728-6738. <https://doi.org/10.1002/mp.15920>
23. Dai T, Sloop AM, Ashraf MR, et al. Commissioning an ultra-high-dose-rate electron linac with end-to-end tests. *Phys Med Biol*. 2024;69(16):165028. <https://doi.org/10.1088/1361-6560/ad69fc>
24. Jaccard M, Duran MT, Petersson K, et al. High dose-per-pulse electron beam dosimetry: Commissioning of the Oriatron eRT6 prototype linear accelerator for preclinical use. *Med Phys*. 2018;45(2):863-874. <https://doi.org/10.1002/mp.12713>
25. Giuliano L, Franciosini G, Palumbo L, et al. Characterization of ultra-high-dose rate electron beams with ElectronFlash linac. *Appl Sci*. 2023;13(1):631. <https://doi.org/10.3390/app13010631>
26. Ashraf MR, Rahman M, Cao X, et al. Individual pulse monitoring and dose control system for pre-clinical implementation of FLASH-RT. *Phys Med Biol*. 2022;67(9):095003. <https://doi.org/10.1088/1361-6560/ac5f6f>
27. Liu K, Holmes S, Schüler E, Beddar S. A comprehensive investigation of the performance of a commercial scintillator system for applications in electron FLASH radiotherapy. *Med Phys*. 2024;51(6):4504-4512. <https://doi.org/10.1002/mp.17030>
28. Poirier Y, Xu J, Mossahebi S, Therriault-Proulx F, Sawant A. Technical note: Characterization and practical applications of a novel plastic scintillator for online dosimetry for an ultrahigh dose rate (FLASH). *Med Phys*. 2022;49(7):4682-4692. <https://doi.org/10.1002/mp.15671>
29. Petersson K, Jaccard M, Germond JF, et al. High dose-per-pulse electron beam dosimetry - A model to correct for the ion recombination in the Advanced Markus ionization chamber. *Med Phys*. 2017;44(3):1157-1167. <https://doi.org/10.1002/mp.12111>
30. Baikalov A, Tho D, Liu K, Bartzsch S, Beddar S, Schüler E. Characterization of a time-resolved, real-time scintillation dosimetry system for ultra-high dose rate radiation therapy applications. *Int J Radiat Oncol Biol Phys*. 2024. <https://doi.org/10.1016/j.ijrobp.2024.11.092>
31. Archambault L, Therriault-Proulx F, Beddar S, Beaulieu L. A mathematical formalism for hyperspectral, multipoint plastic scintillation detectors. *Phys Med Biol*. 2012;57(21):7133-7145. <https://doi.org/10.1088/0031-9155/57/21/7133>

32. Therriault-Proulx F, Archambault L, Beaulieu L, Beddar S. Development of a novel multi-point plastic scintillation detector with a single optical transmission line for radiation dose measurement. *Phys Med Biol.* 2012;57(21):7147-7159. <https://doi.org/10.1088/0031-9155/57/21/7147>
33. Zhou B, Guo L, Lu W, et al. Electron FLASH platform for pre-clinical research: LINAC modification, simplification of pulse control and dosimetry. *arXiv preprint arXiv:240815426.* 2024. <https://doi.org/10.48550/arXiv.2408.15426>
34. Ashraf MR, Rahman M, Zhang R, et al. Dosimetry for FLASH Radiotherapy: A review of tools and the role of radioluminescence and Cherenkov emission. *Front Phys.* 2020;8:328. <https://doi.org/10.3389/fphy.2020.00328>
35. Micke A, Lewis DF, Yu X. Multichannel film dosimetry with nonuniformity correction. *Med Phys.* 2011;38(5):2523-2534. <https://doi.org/10.1118/1.3576105>
36. Therriault-Proulx F, Beaulieu L, Archambault L, Beddar S. On the nature of the light produced within PMMA optical light guides in scintillation fiber-optic dosimetry. *Phys Med Biol.* 2013;58(7):2073-2084. <https://doi.org/10.1088/0031-9155/58/7/2073>
37. Ashraf MR, Bruza P, Krishnaswamy V, Gladstone DJ, Pogue BW. Technical Note: Time-gating to medical linear accelerator pulses: Stray radiation detector. *Med Phys.* 2019;46(2):1044-1048. <https://doi.org/10.1002/mp.13311>
38. Favaudon V, Lentz J-M, Heinrich S, et al. Time-resolved dosimetry of pulsed electron beams in very high dose-rate, FLASH irradiation for radiotherapy preclinical studies. *Nucl Instrum Methods Phys Res, Sect A.* 2019;944:162537. <https://doi.org/10.1016/j.nima.2019.162537>
39. Cecchi DD, Therriault-Proulx F, Lambert-Girard S, et al. Characterization of an x-ray tube-based ultrahigh dose-rate system for in vitro irradiations. *Med Phys.* 2021;48(11):7399-7409. <https://doi.org/10.1002/mp.15234>
40. Vanreusel V, Gasparini A, Galante F, et al. Point scintillator dosimetry in ultra-high dose rate electron "FLASH" radiation therapy: A first characterization. *Phys Med.* 2022;103:127-137. <https://doi.org/10.1016/j.ejmp.2022.10.005>
41. Timakova E, Bazalova-Carter M, Zavgorodni S. Characterization of a 0.8 mm³ Medscint plastic scintillator detector system for small field dosimetry. *Phys Med Biol.* 2023;68(17):175040. <https://doi.org/10.1088/1361-6560/aceacf>
42. Uijtewaal P, Cote B, Foppen T, et al. Performance of the HYPERSCINT scintillation dosimetry research platform for the 1.5 T MR-linac. *Phys Med Biol.* 2023;68(4):04NT01. <https://doi.org/10.1088/1361-6560/acb30c>

43. Beierholm AR, Behrens CF, Andersen CE. Dosimetric characterization of the Exradin W1 plastic scintillator detector through comparison with an in-house developed scintillator system. *Radiat Meas.* 2014;69:50-56. <https://doi.org/10.1016/j.radmeas.2014.08.005>
44. Biagtan E, Goldberg E, Stephens R, Valeroso E, Harmon J. Gamma dose and dose rate effects on scintillator light output. *Nucl Instrum Methods Phys Res, Sect B.* 1996;108(1-2):125-128. [https://doi.org/10.1016/0168-583X\(95\)00874-8](https://doi.org/10.1016/0168-583X(95)00874-8)
45. Giguère C, Hart A, Bateman J, et al. Radiation damage and recovery of plastic scintillators under ultra-high dose rate 200 MeV electrons at CERN CLEAR facility. *arXiv preprint arXiv:241012535.* 2024. <https://doi.org/10.48550/arXiv.2410.12535>
46. Liu K, Palmiero A, Chopra N, et al. Dual beam-current transformer design for monitoring and reporting of electron ultra-high dose rate (FLASH) beam parameters. *J Appl Clin Med Phys.* 2023;24(2):e13891. <https://doi.org/10.1002/acm2.13891>

Supplementary Material

1. Measurement setup and beam parameters

Figure S1 shows the setup of the scintillator measurements for CONV and UHDR irradiation. Unless otherwise stated, all CONV and UHDR measurements were completed based on the setup of Clinac 21EX at 100 cm SSD, 10x10 cm² cone, at 1cm solid water and 1cm bolus depth, and 6 cm solid water backscatter (Fig. S1a). The scintillator probe tip was aligned to the crosshair. The above setup is referred to as the standard setup. A piece of EBT-XD film was directly placed under the scintillator probe for UHDR measurements (Fig. S1b).

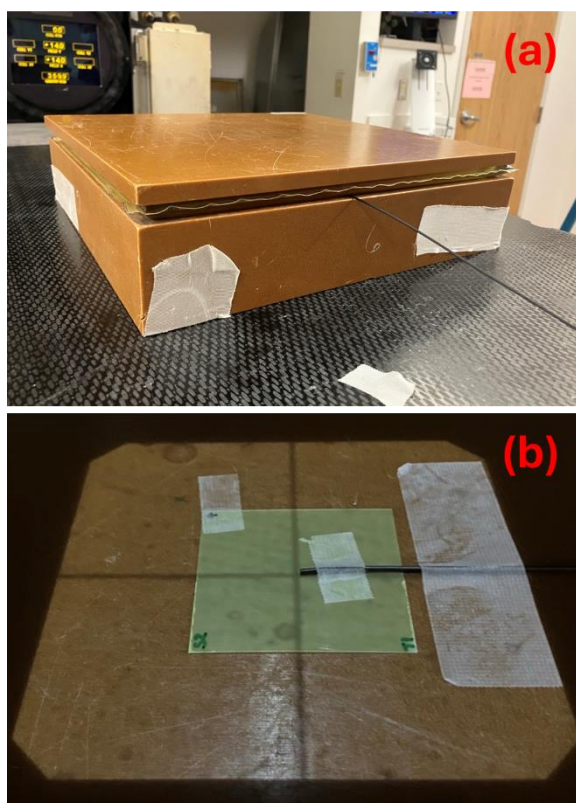


Figure S1. (a) Setup of the scintillator measurements for CONV and UHDR beams. The scintillator is sandwiched between 6 cm solid water backscatter and 1 cm bolus with 1 cm solid water piece on top. The SSD is 100 cm, with a 10x10 cm² cone. (b) For UHDR measurements, a piece of EBT-XD film was directly placed under the scintillator probe.

Table S1 shows the ranges and default values of the irradiation and study parameters of CONV and UHDR beams used throughout our study. The CONV irradiation was only used for dose accuracy studies at a sampling frequency of 1Hz, energy dependence and field size dependence studies, while the 18 MeV UHDR was used for the remaining tests. Unless otherwise specified, the default values were used throughout this study.

Table S1. Ranges and default values of radiation and study parameters.

Symbol	CONV irradiation		UHDR irradiation	
	Range	Default value	Range	Default value
E	6 and 18 MeV	—	—	18 MeV
SSD	—	100 cm	100–140 cm	100 cm
FS	2x2–25x25 cm ²	10x10 cm ²	—	10x10 cm ²
PRF	360 and 180 Hz	—	30–180 Hz	180 Hz
D_{beam}	0–35 Gy	—	0–40 Gy	—
DPP	2.8 x10 ⁻⁴ and 5.6 x10 ⁻⁴ Gy	—	1–2.3 Gy	2.3 Gy
# _{pulse}	—	—	2–17	—
t_{pulse}	—	4.5 μ s	—	4.5 μ s
ADR	—	0.1 Gy/s	—	414 Gy/s
IDR	62 and 123 Gy/s	—	—	5.0 x10 ⁵ Gy/s

Abbreviations: ADR, average dose rate; D_{beam} , absorbed dose; DPP, dose per pulse; E , beam energy; FS, field size; IDR, instantaneous dose rate; PRF, pulse repetition frequency; SSD, source to surface distance; t_{pulse} , pulse width; #_{pulse}, pulse number.

2. Beam energy dependence of the scintillator under 6 and 18 MeV CONV

Table S2 compares the scintillator and IC measurement after receiving 100 MU of 6 and 18 MeV CONV. The chamber measurement was based on the daily outputs measured by the IC, PDD, and water-to-solid water conversion factors. The standard setup was used for this measurement. The uncertainty analysis of scintillator and IC measurements and the relative difference between them consider the measurement uncertainties, as well as a 0.25 mm scintillator depth placement uncertainty quantified by half of the sensitive volume radius, which contributes to the uncertainty in locating PDD for the output calculation. From two-tailed t-test, the detectors' relative reading differences between 6 and 18 MeV have $p = 0.325$, indicating no significant energy dependence observed from the scintillator measurement.

Table S2. Energy dependence of scintillator for 6 and 18 MeV CONV compared to IC

Energy	MU	Scintillator (cGy)	IC measurements				Relative difference
			D_w^Q	% <i>dd</i>	$C_{w \rightarrow sw,d}^Q$	Dose (cGy)	
6 MeV	100	85.36±0.14	100.79	81.75%	1.0176	83.34±1.79	1.81±2.18%
18 MeV	100	100.81±0.11	101.55	99.80%	0.9929	100.63±0.06	0.18±0.13%

Abbreviations: $C_{w \rightarrow sw,d}^Q$, water to solid water conversion factor for beam quality Q at depth d ; D_w^Q , the absorbed dose to water for a given number of MU of beam quality Q ; MU, monitoring units; %*dd*, percent depth dose.

3. Verification of field size factors (f_{FS}) measurement against Varian golden beam data

Figure S2 compares the f_{FS} for 6 and 18 MeV electron beams from 6x6 to 25x25 cm², measured using the Semiflex 31013 IC at 2 cm depth in solid water, or acquired from golden beam data at d_{ref} in water. The measured f_{FS} and the golden beam data agreed within 1%, validating the accuracy of the IC measurements.

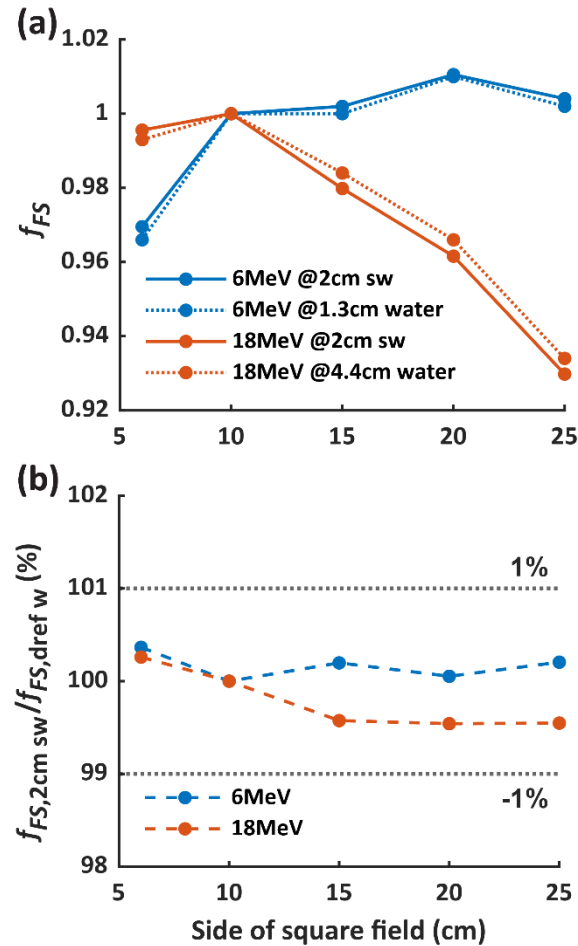


Figure S2. Comparison of field size factors (f_{FS}) for 6 and 18 MeV CONV. (a) shows the f_{FS} measured with IC at depth of 2 cm, and the f_{FS} acquired from golden beam data at d_{ref} in water. (b) shows the ratio of the f_{FS} measured by the IC to those derived from the golden beam data. Abbreviations: f_{FS} , field size factor; w, water; sw, solid water.

4. Effective SSD fitting for 18 MeV at CONV and UHDR

To calculate the dose per pulse (DPP) of the 18 MeV UHDR beam, effective SSD fitting was performed by delivering 4 pulses to the scintillator at 1 Hz, with 1 cm of solid water and 1 cm of bolus as buildup. The square root of the reading ratio at 100 cm SSD and at other SSDs showed good linearity along with SSD ($R^2 > 0.999$, Fig. S3). The DPP at 100 cm SSD was measured directly by the scintillator, while the DPPs at other SSDs were calculated using the effective SSD. For comparison, effective SSD fitting for the 18 MeV CONV beam was also performed by delivering 100 MU to an IC with a 2 cm solid water buildup.

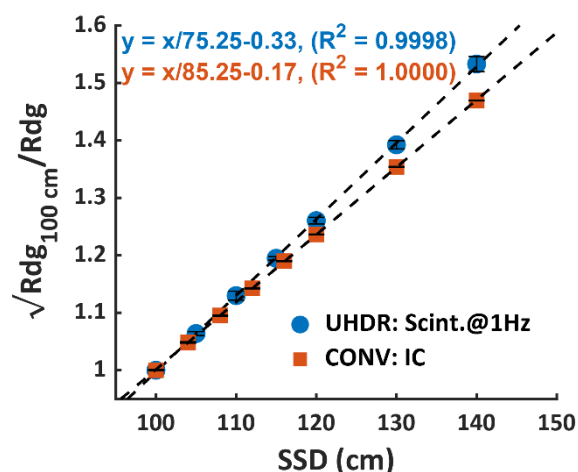


Figure S3. Effective SSD fitting of 18 MeV UHDR and CONV. UHDR measurements were performed by delivering 4 pulses of 18 MeV UHDR to the scintillator at 1 Hz, with 1 cm of solid water and 1 cm of bolus as buildup. CONV measurements were performed by delivering 100 MU of 18 MeV CONV to an IC with a 2 cm solid water buildup.

5. Pulse repetition frequency (PRF) measurement with a remote trigger unit

To assess the pulse repetition frequency of the 18 MeV UHDR delivery, the remote trigger unit (RTU, described in Section 2.8) was positioned outside the radiation field to detect scattered radiation. Four pulses were delivered at 100, 200, 300, and 600 MU/min. As shown in Fig. S4, the PRF corresponded to 30, 60, 90, and 180 Hz, respectively.

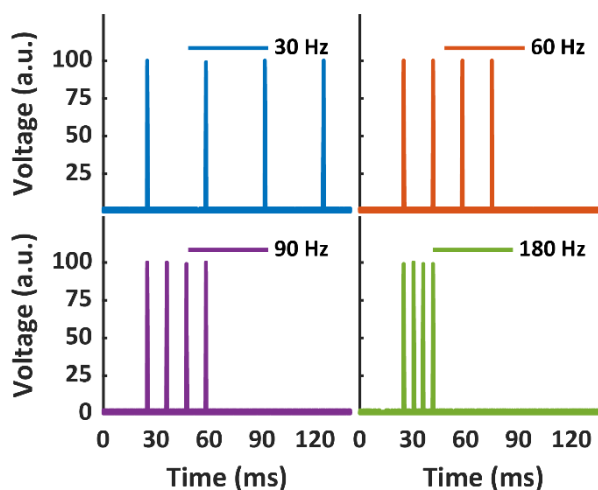


Figure S4. Pulse repetition frequency validated by the remote trigger unit. Four 18 MeV UHDR beams were delivered at 100, 200, 300, and 600 MU/min, with corresponding PRF of 30, 60, 90, and 180 Hz, respectively.

6. Determination of accumulated dose to scintillator using CC13

To determine the accumulated dose delivered to the scintillator, a CC13 was placed at the edge of the cone (Fig. S5a) to measure both Bremsstrahlung and scatter radiation. Due to the relatively low dose rate of the Bremsstrahlung and scatter radiation, as well as the small sensitive volume of the CC13 chamber (0.13 cm^3), the CC13 readings showed linearity with the dose delivered to the scintillator up to 40 Gy (Fig. S5b).

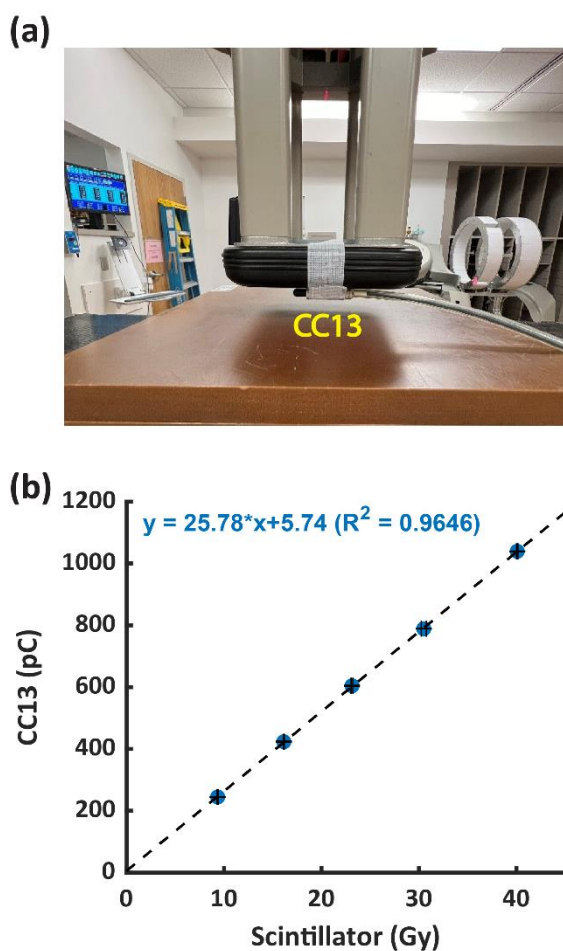


Figure S5. A CC13 was used to determine the accumulated dose to the scintillator. (a) shows the CC13 placed under the edge of the cone. (b) shows that the CC13 signal exhibits a linear relationship with the scintillator reading.